Earth Surface Processes and Landforms
Earth Surf. Process. Landforms **30**, 1203–1225 (2005)
Published online in Wiley InterScience (www.interscience.wiley.com). **DOI:** 10.1002/esp.1271

Constraints on the rate of post-orogenic erosional decay from low-temperature thermochronological data: application to the Dabie Shan, China

Jean Braun[1]* and Xavier Robert[2]

[1] *Research School of Earth Sciences, The Australian National University, Canberra ACT 0200, Australia. Now at Géosciences Rennes, Université de Rennes 1, Rennes, France*

[2] *Département de Géologie, Ecole Normale Supérieure, Lyon, France. Now at Laboratoire de Géodynamique des Chaînes Alpines, Université Joseph Fourier, Grenoble, France*

**Correspondence to: J. Braun, Géosciences Rennes, Université de Rennes 1, Av. Gl Lectere, Rennes 35042, France. E-mail: Jean.Braun@univ-rennes1.fr*

Received 1 September 2004;
Revised 1 March 2005;
Accepted 17 March 2005

Abstract

We have investigated whether low temperature thermochronological datasets can be used to constrain the rate of surface evolution during the post-orogenic phase of a mountain belt. We use a numerical method to solve the heat transport equation in the Earth's crust, including the effects of a changing, finite-amplitude topography and the resulting flexural isostatic rebound. We demonstrate that accurate estimates of the amount of relief loss can be obtained by applying a recently developed spectral method that is based on estimates of the relationship between age and surface elevation as a function of topographic wavelength. We also show that the rate at which topography decays with time following cessation of tectonic activity can be constrained from estimates of exhumation rate derived from the slope of age–elevation profiles collected across short wavelength topography. Using the Neighbourhood Algorithm to perform a thorough search through parameter space, we are able to find a tectonomorphic scenario that predicts age distributions compatible with a thermochronological dataset collected in the Dabie Shan of eastern China by Reiners *et al.* (*American Journal of Science* 2003, vol. 303, pp. 489–518). We demonstrate that, in the Dabie Shan, the mean topographic relief has decreased by a factor of 2·5 to 4·5 during the last 60–80 Ma, while the mountain belt experienced a mean exhumation rate of 0·01 to 0·04 km Ma^{-1}. We confirm the conclusions of Reiners *et al.* that there is no need to invoke a discrete Cenozoic tectonic event to explain the observed age distribution. The thermochronological dataset can also be used to put constraints on the effective elastic thickness of the lithosphere underlying the orogen (10 to 30 km). There is, however, a trade-off between elastic thickness, mean exhumation rate and amount of topographic relief loss. The most likely scenario also predicts that the topography has decreased at a constant rate since the end of orogenic activity about 100 Ma ago. Copyright © 2005 John Wiley & Sons, Ltd.

Keywords: thermochronology; erosion; Dabie Shan; flexure

Introduction

It is well known that the rate at which landscapes evolve with time is strongly dependent on the local tectonic forcing (Kooi and Beaumont, 1996). The classical concepts of dynamic equilibrium landforms (Hack, 1960), phases of growth and decay of relief (Penck, 1924), and relaxation of landforms (Davis, 1899) can be understood as different aspects of the behaviour of the coupled tectonic–erosion system (Kooi and Beaumont, 1996). This is because, at the scale of an orogen, erosional processes can be characterized by a typical timescale (or rate at which they take place), the 'erosional response time' (Kooi and Beaumont, 1996). The erosional response time of an orogen depends on its geometry, i.e. its height, extent and overal shape, but also on the local climate and on the nature of the dominant process(es) for erosion (fluvial, glacial or hillsope processes, for example) (Kooi and Beaumont, 1996; Lague *et al.*, 2003; Whipple and Tucker, 1999).

In areas of slow tectonic forcing, erosion processes are usually capable of rapidly achieving a steady state in which the tectonic flux, i.e. the rate of mass input into an orogenic area, is perfectly compensated by the erosional flux, i.e. the removal of mass by erosion and transport (Kooi and Beaumont, 1996). In cases where the tectonic forcing takes place over a timescale that is similar to the erosional response time of the system, the erosional flux is always out of phase with respect to the tectonic flux (Kooi and Beaumont, 1996). However, when an orogen is subjected to a very rapid or discrete tectonic event, the erosional response takes the form of an exponential decay at a rate directly determined by the erosional response time (Kooi and Beaumont, 1996). Consequently, the erosional decay of a mountain belt that follows cessation of tectonic activity, usually in response to a discrete event of plate reorganization, provides us with an opportunity to determine the erosional response time of orogenic systems.

Erosion causes rocks to be advected towards the surface and cool. The timing of this cooling can be well constrained by thermochronology. In essence, for a given thermochronological system, the 'age' of a rock corresponds to the time at which it cooled through a so-called 'closure temperature' (Dodson, 1973). Dating rocks should therefore provide us with good estimates on the rate at which rocks are brought to the surface and, consequently, with good constraints on the rate at which surface erosion takes place. The purpose of the work described here is to demonstrate whether one can extract useful information from thermochronological datasets about the evolution of surface topography during the post-orogenic phase of a mountain belt.

It is, however, important to realize that surface erosion and transport in a 'tectonically quiet' area causes the underlying lithosphere to 'rebound' by isostasy (Molnar and England, 1990; Montgomery, 1994) at a scale that is determined by the flexural strength of the underlying lithosphere. This orogen-wide uplift causes further surface erosion. Thus, to use thermochronological data to quantify the rate of surface erosion and, from it, derive an estimate of the rate of relief evolution, one needs to incorporate the effect of isostasy.

In this paper, we first discuss the isostatic rebound associated with the evolution of surface topography by erosional processes. We consider the importance of the lithosphere flexural strength on the isostatic response of the system to erosion. Using a numerical method to solve the heat transport equation in three dimensions, we show how a synthetic age distribution can be computed and how it is affected by our assumption about the isostatic response of the lithosphere to surface unloading. We then investigate whether the age distribution is sensitive to the assumed erosional response time. Finally we use an inversion method to extract information on the rate of surface relief evolution in the Dabie Shan, from a thermochronological dataset collected by Reiners *et al*. (2003) in the area.

Local Isostasy

The post-orogenic phase of most mountain belts is characterized by a gradual erosion of the relief/topography created during the active tectonic phase. This erosion results in unloading of the underlying lithosphere and subsequent isostatic adjustment. The principle of isostasy states that there is a region beneath the lithosphere where rocks are so weak that they cannot sustain any horizontal stress gradient over geological times (i.e. greater than a few tens of thousands of years). This implies that, at isostatic equilibrium, the weight of adjacent lithospheric columns must be equal. Erosion of surface topography results in a reduction of the weight of the underlying lithospheric column and must therefore be compensated by vertical uplift.

As shown in Figure 1, surface erosion by an amount E_0 (panel b) of a reference lithospheric column (panel a) of crustal thickness h and total thickness $h + L$ results in an isostatic surface uplift by an amount u (panel c) such that the weights of the two columns (a and c) down to the compensation depth $h + L + d$ are identical. This leads to the following relationship:

$$h\rho_c + L\rho_m + d\rho_a = (h - E_0)\rho_c + L\rho_m + (d + u)\rho_a \tag{1}$$

where ρ_c, ρ_m and ρ_a are the mean densities of the crust, mantle lithosphere and asthenosphere, respectively, from which an expression for the isostatic uplift u as a function of the erosion, E_0, can be derived:

$$u = E_0 \frac{\rho_c}{\rho_a} \tag{2}$$

From this relationship, one can also derive the expression for the amount of erosion, E, needed to reduce topography by an amount Δh:

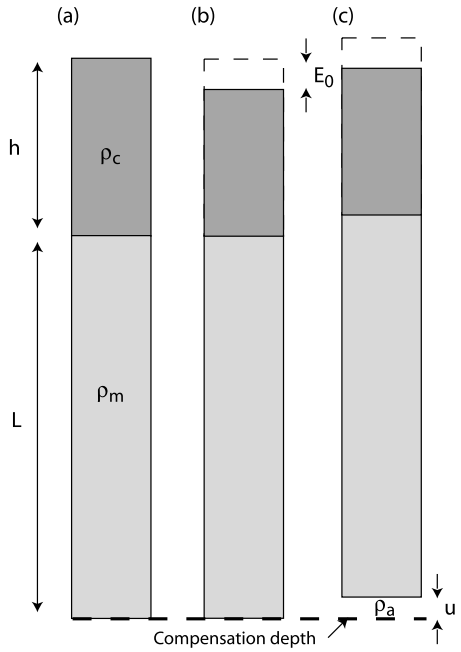

Figure 1. Erosion at the surface of a reference lithospheric column (a) by an amount E_0 (b) leads to isostatic uplift of the column by an amount u (c). For typical density and crustal thickness values, $u = 4$ to $5 \times E_0$.

$$E = \frac{\Delta h}{1 - \dfrac{\rho_c}{\rho_a}} \tag{3}$$

which, for average values of upper crustal and asthenospheric densities of 2600 and 3200 kg m^{-3}, respectively, leads to an isostatic amplification factor of approximately 5·3. This means that for every kilometre of surface topography reduction, one needs to erode approximately 5·3 km of crustal rocks. This also means that during the post-orogenic phase of a mountain belt, erosion of the topography may lead to tens of kilometres of exhumation, rock cooling and the subsequent closure of thermochronological systems, especially those characterized by a low closure temperature, such as apatite (U-Th)/He dating or apatite fission track dating. Consequently, for those thermochronological systems, ages observed at the surface of an ancient mountain belt are more likely to provide information about the rate of erosion and surface relief evolution during the post-orogenic phase of the mountain belt than about the rate of tectonic uplift and exhumation during its constructive (or orogenic) phase.

Flexural Isostasy

The concept of an 'isostatic compensation depth' leads to a vertically integrated mass balance only if one neglects the lateral strength of the lithosphere. This is usually true for very wide load, i.e. loads that are much wider than the thickness of the lithosphere. However, the load associated with erosional processes at the scale of a single valley or mountain range (1 to 100 km) is typically narrower than the thickness of the continental lithosphere (typically ranging from a few kilometres to several hundred kilometres).

The lateral strength of the continental lithosphere is usually taken into account by parameterizing its isostatic response as that of a thin, yet strong, elastic plate 'floating' on the underlying inviscid asthenosphere (Turcotte, 1979). Under the assumption that the surface deflection of the lithosphere, w, is small in comparison to its thickness, one can derive the following partial differential equation that relates w to an applied distributed vertical surface load, $q(x)$:

$$D\frac{\partial^4 w}{\partial x^4} + (\rho_a - \rho_s)gw = q(x) \tag{4}$$

where x is the horizontal spatial coordinate, D is the flexural rigidity of the plate, ρ_a and ρ_s are the densities of the asthenosphere and sediment/crust/air, respectively, and g is gravitational acceleration (Turcotte, 1979). What ρ_s represents depends on the assumption made on the evolution of the surface following its deflection by elastic rebound: if subsidence is accompanied by sedimentation, ρ_s is sediment density; if no sedimentation takes place, ρ_s is water density; where the surface is uplifted but no erosion takes place, ρ_s should be upper crustal rock density; where the surface is uplifted and erosion is very efficient, ρ_s should be zero.

The flexural rigidity can be expressed in terms of the elastic constants, Y_m and ν (Young's modulus and Poisson's ratio), and the assumed elastic thickness of the plate, L_e (Turcotte, 1979):

$$D = \frac{Y_m L_e^3}{12(1-\nu^2)} \tag{5}$$

Periodic Loading

The flexural isostatic response of the lithosphere to a periodic surface load (resulting, for example, from a periodic surface topography of amplitude h_0 and wavelength λ) can be obtained from the solution of Equation 4 in which:

$$q(x) = \rho_c g h_0 \sin\frac{2\pi x}{\lambda} \tag{6}$$

The solution is in phase with the load:

$$w = w_0 \sin\frac{2\pi x}{\lambda} \tag{7}$$

and its amplitude, w_0, is given by:

$$w_0 = \frac{h_0}{\frac{\rho_a}{\rho_c} - 1 + \frac{D}{\rho_c g}\left(\frac{2\pi}{\lambda}\right)^4} \tag{8}$$

The amplitude of the deformation depends on the wavelength of the load, λ, compared to the flexural wavelength, x_α, given by:

$$x_a = \left(\frac{D}{\rho_c g}\right)^{\frac{1}{4}} \tag{9}$$

Two end-member cases exist. First, when the wavelength of the topography is small in comparison to the flexural wavelength

$$\lambda << x_\alpha \tag{10}$$

the deflection of the plate, and thus the isostatic response of the lithosphere, becomes neglegible in comparison to the amplitude of the surface topography:

$$w_0 << h_0 \tag{11}$$

This means that the load of the topography is small enough to be fully compensated by the flexural strength of the lithosphere. Second, in cases where the wavelength of the topography is much greater than the flexural wavelength

$$\lambda >> x_\alpha \tag{12}$$

the flexural strength of the lithosphere becomes negligible and the topography is in local isostatic equilibrium:

$$w_0 = \frac{\rho_c h_0}{\rho_a - \rho_c} = w_0^e \tag{13}$$

The degree of isostatic compensation, C, of a topographic load of wavelength λ is defined as the ratio of the deflection of the lithosphere (Equation 13) to its maximum local isostatic (or hydrostatic) deflection (Equation 8):

$$C = \frac{w_0}{w_0^e} = C = \frac{\rho_a - \rho_c}{\rho_a - \rho_c + \frac{D}{g}\left(\frac{2\pi}{\lambda}\right)^4} \tag{14}$$

For small wavelength topography ($\lambda << x_\alpha$), C tends towards 0; for long wavelength topography ($\lambda >> x_\alpha$), C tends towards 1.

Isostatic Response to Relief Reduction

Whether topography is in isostatic equilibrium or fully compensated by the lateral strength of the lithosphere will affect the amount of isostatic amplification associated with post-orogenic relief reduction by erosion. To follow the convention of Braun (2002a), we will assume that today's topographic amplitude is β times what it was at the end of the orogenic phase (i.e. before the post-orogenic decay started). The change in surface topography is given by:

$$\Delta h = \left(\frac{1}{\beta} - 1\right) h_0 \tag{15}$$

where h_0 is the initial topography. Using Equation 8, Equation 3 can be generalized to obtain the total erosion, E, necessary to achieve a change in topography, Δh, at a wavelength λ, taking into account the flexural response of the lithosphere:

$$\begin{aligned} E &= \left(\frac{1}{\beta} - 1\right) h_0 + \left(\frac{1}{\beta} - 1\right) h_0 \frac{\rho_c}{\rho_a - \rho_c} C \\ &= \left(\frac{1}{\beta} - 1\right) h_0 \left(1 + \frac{\rho_c}{\rho_a - \rho_c} C\right) \end{aligned} \tag{16}$$

E tends towards the local isostatic solution (Equation 3) when C tends towards 1 (long wavelength topographic change); E tends towards the change in surface topography, Δh, when C tends towards 0 (short wavelength topographic change).

Topography Spectral Content and Age–Elevation Gain Function

Surface topography in active orogenic belts is typically characterized by a range of wavelengths, from small-scale relief at the valley scale to large-scale relief at the mountain belt scale (Huang and Turcotte, 1989). As suggested by (Braun, 2002a), this relatively wide spectrum of surface topography amplitude can be used to extract meaningful information about mean exhumation rate and the rate of surface topography change from thermochronological datasets. Indeed, the penetration depth of the thermal perturbation caused by finite amplitude surface topography decays exponentially with the wavelength of the topography (Turcotte and Schubert, 1982). Isotherms thus tend to follow the shape of the long wavelength component of the topography, while they are unaffected by the short wavelength component. This, in turn, implies that age–elevation relationships measured along very steep topographic profile provide a good estimate of the mean exhumation rate, while age–elevation relationships measured over long distances (i.e. of the same order as the longest wavelength in the topographic signal) provide a good estimate of the rate of change of the amplitude of the topography (Braun, 2002a).

A spectral method can be used to extract this information from age profiles collected along linear transects that (a) sample the surface topography at a wide range of wavelengths and (b) are orientated in such a way that the mean exhumation rate is relatively constant along the transect (Braun, 2002a). Optimally, such transects should contain up to several tens of regularly spaced points, be located in the part of the mountain belt characterized by the highest topographic

relief and orientated in a way that the mean exhumation rate is uniform along the transect and that the transect is perpendicular to drainage direction (i.e. mean local slope). Age–elevation data collected along the transect can then be used to build a gain function, G, that describes the relationship between age and elevation as a function of the wavelength of the topography, λ. The gain function can be constructed following classical spectral analysis methods (Jenkins and Watts, 1968) from an input signal (here the topographic profile) and an output signal (here the age dataset):

$$G(\lambda) = \frac{\sqrt{C_{12}^2 + Q_{12}^2}}{C_{11}} \tag{17}$$

where C_{12} and Q_{12} are the real and imaginary parts of the cross-spectrum obtained from the real and imaginary parts of the smoothed spectral estimators of the input and output signals. These estimators are, in turn, obtained from the Fourier transforms of the windowed input (elevation, z) and output (age, a) signals, R_z, I_z and R_a, I_a (Jenkins and Watts, 1968):

$$\begin{aligned} C_{12} &= R_z R_a + I_z I_a \\ Q_{12} &= I_z R_a - R_z I_a \end{aligned} \tag{18}$$

C_{11} is the power spectrum of the input signal:

$$C_{11} = R_z^2 + I_z^2 \tag{19}$$

The smoothed spectral estimators are obtained by applying a triangular Bartlett window (see Jenkins and Watts, 1968, p. 244) to the elevation and age profiles prior to the calculation of the Fourier transforms. Confidence intervals can be calculated from the smooth spectral estimators (see Jenkins and Watts, 1968, p. 437).

At short wavelengths, gain estimates (G_S) are inversely proportional to the mean exhumation rate; at long wavelengths, gain estimates (G_L) contain information on the change in surface topography amplitude (relief), β, over a time equal to the mean value of the age dataset:

$$\beta = \frac{1}{1 - \dfrac{G_L}{G_S}} \tag{20}$$

The derivation of this important relationship as well as more information on the use of the spectral method to interpret age–elevation datasets can be found in Braun (2002a).

Here, we propose to determine whether the spectral method can be used to estimate the mean rate of exhumation and the rate of topographic change during the post-orogenic phase in the evolution of a mountain belt. In such a situation, the rate of change of the geometry of the surface by surface erosion is also controlling the mean exhumation rate of the area through isostatic compensation. Thus, the two signals that we are trying to deconvolve by spectral analysis, are, in fact, spatially correlated at a wavelength that is determined by the flexural properties of the underlying lithosphere.

Effect on Age Distribution

To demonstrate this point, we first use a numerical model solving the heat transfer equation to investigate the effect of erosion-driven isostatic rebound on the distribution of ages measured along the surface of an old orogenic belt. The model is a modified version of the Pecube software, developed by Braun (2003), in which we have incorporated a module to calculate the vertical surface deflection of a thin elastic plate due to an applied surface vertical load, using the spectral method described in Nunn and Aires (1988). Pecube is a finite element code solving the heat transport equation in three dimensions:

$$\frac{\partial T}{\partial t} + \dot{E}\frac{\partial T}{\partial z} = \kappa\frac{\partial^2 T}{\partial x^2} + \kappa\frac{\partial^2 T}{\partial y^2} + \kappa\frac{\partial^2 T}{\partial z^2} + \frac{H}{c} \tag{21}$$

including the effects of vertical heat advection due to erosion ($\dot{E}$), heat conduction and heat production. T is temperature, x, y and z are spatial coordinates, t is time, k is thermal diffusivity, H is the rate of heat production per unit mass

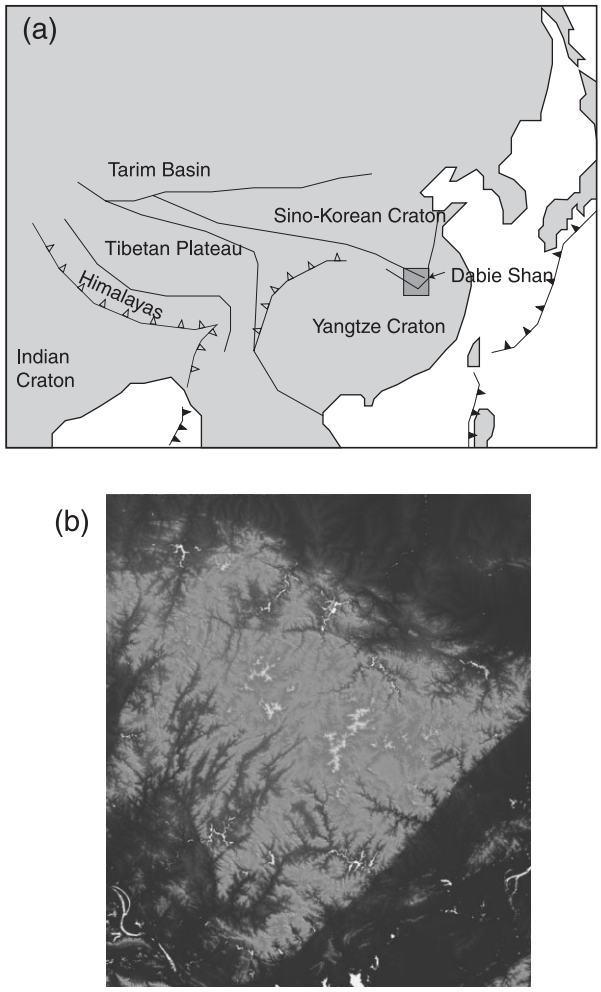

Figure 2. (a) Location of major tectonic elements surrounding the Dabie Shan and (b) topographic data used in this study.

and c is heat capacity. Pecube has been designed to accurately predict the effect of a finite amplitude, time-varying surface topography on the underlying temperature structure. More details on Pecube can be found in Braun (2003). Flexural isostasy has been included by computing at each time step, from the imposed change in surface topography, Δh, the resulting negative load, $\rho_c g \Delta h \times \Delta x \Delta y$, and the ensuing isostatic uplift. This uplift is then imposed as a velocity term in a system of reference that is fixed with respect to the base of the model.

Rather than using a synthetic topographic surface, we have used a topographic dataset from the Dabie Shan area in southeastern China (Figure 2a). The reason for this particular choice of natural topography is that we also have access to a rather extensive thermochronological dataset for this area (Reiners *et al*., 2003). This orogen developed between the northern edge of the Yantze craton and the southeastern corner of the Sino-Korean craton during a series of subduction-related episodes of crustal shortening, from the late Palaeozoic to the mid-Cretaceous (Schmid *et al*., 2001). There is debate on whether the orogen was reactivated during the ongoing Indo-Asian collision and whether some of the present-day topographic relief is the result of this Cenozoic reactivation (Grimmer *et al*., 2002). Alternatively, the topography is the erosional remnant of a much larger amplitude relief that was entirely formed in the Cretaceous (Reiners *et al*., 2003).

Later in this paper, we will make use of the thermochronological data to extract from them quantitative estimates of the amount of post-orogenic topographic decay and its timing. In a first step, however, we will use the topography of this area (a 190 by 220 km rectangular section extracted from the 30 arc second resolution DEM GTOPO30; Figure 2b) in a series of model runs in which we investigate the effect on low-T age distributions of the isostatic

rebound associated with a post-orogenic erosional phase. To perform this sensitivity analysis, we first impose that the topographic relief was arbitrarily four times larger 100 Ma ago than it is today and that it has decayed linearly since then, to reach its present-day value at the end of the model run. Changes in surface relief are imposed by changing the amplitude of the topography, not its shape. This is an approximation that is likely to be correct in a setting where horizontal tectonic advection is not important, such as during the post-orogenic phase of a mountain belt. In these situations, the potential for stream capture and reorganization of the drainage network is indeed small. It is, however, likely that the small-scale diffusive processes acting along hillslopes will decrease small-scale relief first and, in principle, one should assume a faster removal of the small-scale components of relief in comparison to its large-scale features. Hillslope processes are, however, active on a scale (tens to hundreds of metres) that is well below the horizontal scale of the topographic effects recorded by thermochronology.

We have first performed a series of five model runs to investigate how sensitive the predicted ages are to the assumed elastic plate thickness. The model runs differ by the assumed elastic plate thicknesses, 0, 1, 10, 20 and 40 km, which correspond to flexural wavelengths of 0, 4·1, 23, 39 and 66 km, respectively, if one assumes that $Y_m = 10^{11}$ Pa, $\nu = 0{\cdot}25$ and $\rho_c g = 3 \times 10^4$ Pa m^{-1}. The apatite He ages are computed from temperature–time histories derived from the results of the Pecube model using the method described by Wolf *et al*. (1998). We do not specify an *a priori* closure temperature for the (U-Th)/He system in apatite; the temperature range across which the system will 'close' is internally determined, including the effect of cooling rate and diffusion domain size. A temperature of 600 °C is imposed at the base of the model, 30 km beneath the surface. Note that, although there is a likely relationship between the effective elastic plate thickness and the thermal structure of the lithosphere, here we have assumed that these two parameters are independent. Heat diffusivity is set at 25 km^2 Ma^{-1}. Temperature at the surface, T_s, is imposed to be proportional to topographic height, h, according to:

$$T_s = T_{msl} + \gamma h \tag{22}$$

where T_{msl} is temperature at mean sea level ($z = 0$) and is taken to be 10 °C, and γ is the lapse rate (4 °C km^{-1}), i.e. the rate of decrease of temperature with elevation in the atmosphere. Heat production over heat capacity, H/c, is uniform throughout the crust and set at 8 °C Ma^{-1}. The initial temperature structure is assumed to be at equilibrium (steady state) with the imposed boundary conditions. We performed several model runs in which the initial temperature structure was first calculated assuming a mean exhumation rate of 1 km Ma^{-1} to represent the active tectonic phase preceding the post-orogenic decay phase of the orogen, but found that it did not affect the results in a significant way.

The results of five model experiments are shown in Figure 3 as five predicted apatite (U-Th)/He age distributions across the strike of the orogen, from the northwest to the southeast. In all model runs, ages are young near the centre of the orogen (Figure 3), i.e. they are smaller than the length of the model run (100 Ma). We have chosen the mean geothermal gradient (600/30 = 20 °C km^{-1}) and the amount of topographic relief reduction ($\beta^{-1} = 4$) such that, even in the absence of isostatic rebound, rocks that end up at the surface of the model have a starting temperature well above the apatite He closure temperature, typically in the range 55–75 °C, and see their age set during the post-orogenic exhumation. The minimum reset ages, found near the centre of the orogen, are inversely proportional to the assumed elastic plate thickness. Because we have assumed that the rate of decrease in surface topographic relief is constant through time, the larger the total erosion, the younger the ages. For low values of the elastic plate thickness (0–1 km), the system is at or near local isostatic equilibrium and the reduction in surface topographic relief over the last 100 Ma causes very large (up to 6 km) isostatic rebound and erosion. As the elastic plate thickness is increased, the amount of isostatic rebound decreases and the total amount of erosion necessary to reduce the surface topographic relief by a factor of 4 decreases.

Effect on Age–Elevation Distributions

A different way to look at these results is to state that, on the scale on the orogen, the ages are inversely proportional to (present-day) elevation, i.e. ages are younger near the centre of the orogen where topography is currently the largest. However, if one looks at the relationship between age and elevation at the scale of an individual valley (10 km in length), three behaviours are observed (Figure 3). In cases where the flexural wavelength is larger than the width of the valleys ($L_e = 10$, 20, 40 km), there is a strong positive correlation between age and elevation; in the case where the flexural wavelength is similar to the width of the smallest valleys ($L_e = 1$ km), there is little variation in age with elevation; in the case where the flexural wavelength is smaller than the valley width ($L_e = 0$ km), predicted age is inversely proportional to elevation.

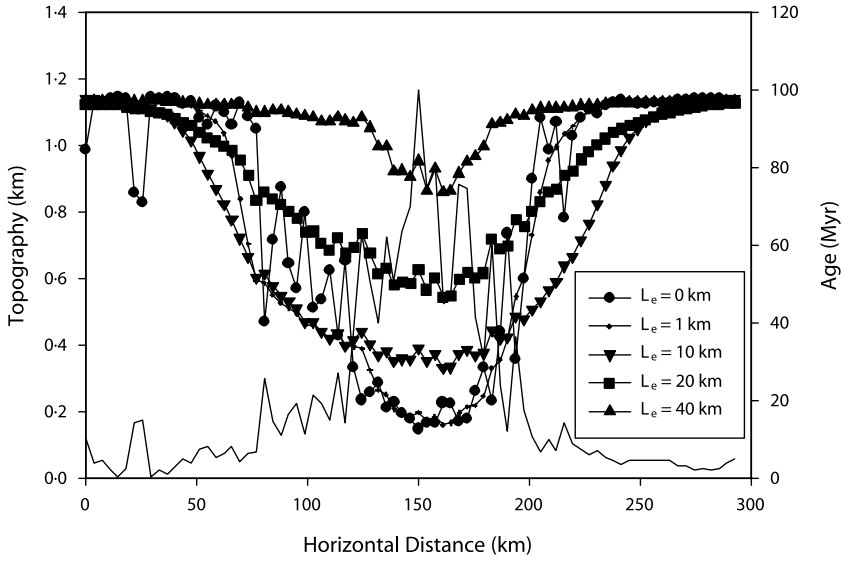

Figure 3. Topography and computed apatite He ages along a profile crossing the study area from the northwest to the southeast assuming different values for the elastic plate thickness.

This behaviour of the coupled erosional–isostatic system can be further documented by computing age–elevation profiles in two separate valleys, one near the centre of the orogen, the other half-way between the centre and one of its margins. Computed age–elevation profiles are shown in Figure 4. In both locations, the slope of the age–elevation relationship is negative when the flexural wavelength is very small and positive otherwise. When the elastic plate thickness is finite, the slope decreases with increasing elastic plate thickness. These synthetic transects are 'collected' across topographic features characterized by a wavelength (10 km) that is moderately larger than the critical wavelength, λ_c, given by the ratio of the closure temperature for the thermochronological system considered (55–75 °C) and geothermal gradient (20 °C km^{-1}) (Braun, 2002a). The perturbation caused by the valleys on the closure temperature isotherm is therefore moderate and the slope of the age–elevation profiles should provide a reasonable, yet overestimated measure of the local erosion rate (Braun, 2002a,b; Stüwe *et al.*, 1994). In the case where the elastic thickness is large ($L_e = 20$ or 40 km) and isostatic rebound is negligible, total erosion is equal to the change in topographic amplitude (3 km near the centre of the orogen and 1·5 km near its margin) and the mean exhumation rate should be of the order of 0·03 or 0·015 km Ma^{-1}, respectively. The slope of the age–elevation relationship is 0·085 and 0·071 km Ma^{-1} near the centre of the orogen, for $L_e = 20$ and 40 km, respectively, and 0·041 and 0·087 km Ma^{-1} near the margin. When isostatic rebound becomes important (i.e. for smaller values of the assumed elastic plate thickness), the total erosion and, consequently, the mean erosion rate increase. This is why the model predicts that the apparent erosion rate derived from the slope of the age–elevation relationship measured along narrow valley profiles increases with decreasing elastic plate thickness.

Estimates of Relief Change Based on the Spectral Method

The results of these five model runs can also be used to determine under which circumstances the spectral method developed by Braun (2002a) can be used to estimate the amount of relief change experienced during the post-orogenic erosional decay of an ancient mountain belt. We first calculate the spectral content of the topographic profile along which age estimates will be used to determine the gain function. The results are shown in Figure 5 and demonstrate that the topographic profile is made of a long wavelength (approximately 150 km) component and a series of shorter wavelength components, the smallest above noise level is at approximately 12 km. We then estimate the value of the gain function between topography and age (G) at those two wavelengths and use them to compute the apparent change in topographic relief based on Equation 20.

To estimate the gain values G_L and G_S, we compute the power spectra of the topography and the predicted ages and combine their real and imaginary parts as detailed in Braun (2002a). We use two different methods to estimate

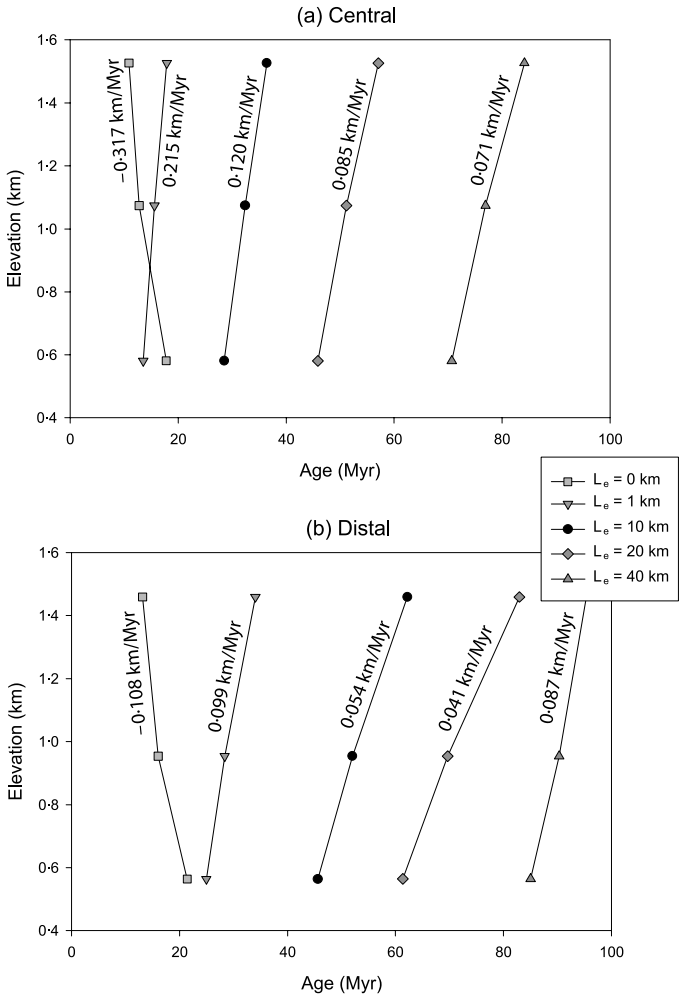

Figure 4. Computed apatite He age–elevation profiles along two 10-km-wide valleys, one near the centre of the orogen (a) and the other one half-way between the centre of the orogen and one of its margins (b). Each profile corresponds to a different value for the assumed elastic thickness, L_e.

the power spectra. The first method makes use of a Bartlett window, the second is based on multiple estimates of the spectrum from sub-samples of the topographic and age profiles which are then used to determine a mean value and standard deviation of the gain function at both wavelengths. The results are summarized in Table I. They demonstrate that the spectral method provides very good estimates of the topographic amplitude change when the plate thickness is of the order of 10 km or more. More generally, one can state that the spectral method can be used in situations where the degree of isostatic compensation, C, of the orogen is less than 0·5. For larger degrees of compensation (or smaller plate thicknesses), one of the main assumptions on which the spectral method is based is violated: the isostatic uplift and thus the mean erosion rate is not uniform across the orogen; in the case of local isostasy ($C = 1$), total erosion is directly proportional to topography and ages are inversely correlated to elevation, at all wavelengths.

Estimates of the elastic thickness of the continental lithosphere vary from a few to several hundred kilometres (Forsyth, 1985). In many cratonic areas, i.e. those which have not been subjected to a recent tectonic event, L_e estimates are consistently larger than 10 km (Bechtel *et al*., 1990; Maggi *et al*., 2000; Wang and Mareschal, 1999; Zuber *et al*., 1989). It is thus clear that the spectral method is likely to provide accurate estimates of topographic relief change associated with the erosional decay of ancient mountain belts.

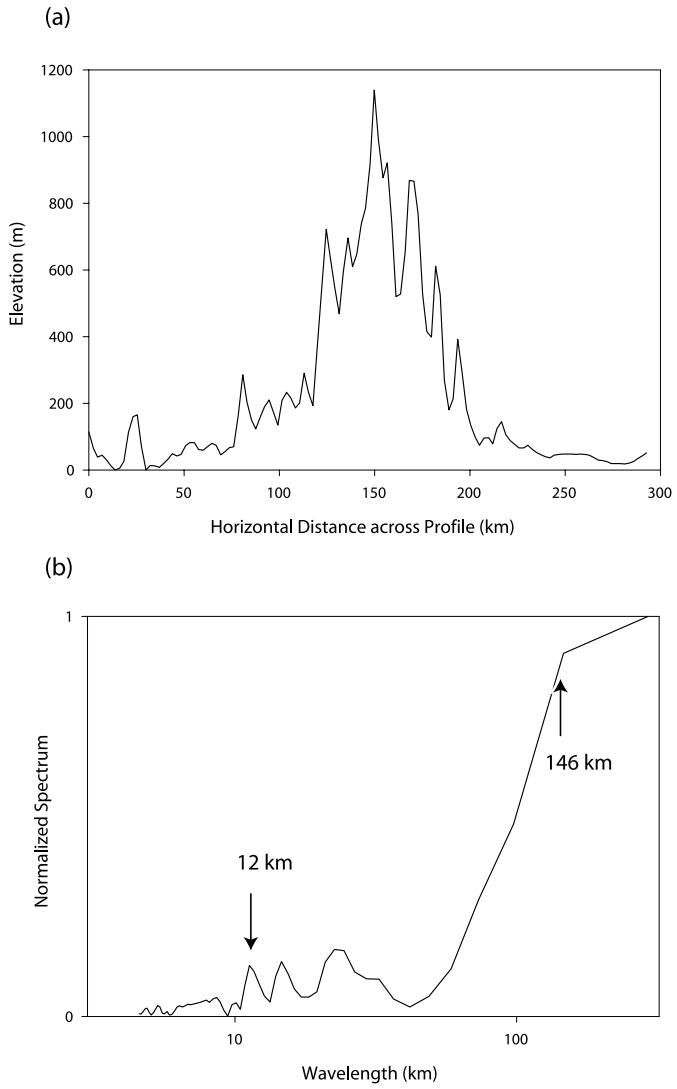

Figure 5. Topographic profile used to calculate the gain function (a) and its power spectrum (b). The arrows point to the components of the spectrum where the long wavelength gain value, G_L, and short wavelength gain value, G_S, are estimated to determine the amplitude of the relief loss (β^{-1}).

Table I. Computed gain values, G_L and G_S, and corresponding relief loss amplitude, β^{-1}, for five model runs characterized by different values of the elastic plate thickness, L_e. Method 1 is based on filtering of the age and elevation data by a Bartlett window. Method 2 is based on multiple computations of the gain function from sub-samples of the age and elevation datasets to derive error estimates

	Method 1			Method 2		
L_e (km)	G_L (Ma km^{-1})	G_S (Ma km^{-1})	β^{-1}	G_L (Ma km^{-1})	G_S (Ma km^{-1})	β^{-1}
0	–98	–27·1	–2·6	–106 ± 2	–58 ± 3	–0·83
1	–81	8·7	10·3	–94 ± 3	8·4 ± 4	12·2
10	–36	10·4	4·5	–51 ± 2	10·3 ± 3	5·9
20	–38	15·3	3·5	–45 ± 1	15·6 ± 2	3·9
40	–23	10·57	3·2	–23 ± 2	9·4 ± 1	3·4

Erosional Response Time

Now that we have established that, under most circumstances, the relief reduction accompanying the erosion decay of ancient mountain belts can be accurately derived from age–elevation datasets, we turn to the question of timing. Clearly, relief reduction estimates can be used to derive a minimum estimate for the rate of relief evolution, by assuming that the rate of erosion has been constant through time since the end of the orogenic phase. As most geomorphic laws imply that the rate of erosion should be somehow proportional to the height of the mountain belt (Whipple and Tucker, 1999), either through a slope or curvature dependence, it is most likely that relief evolution during a post-orogenic 'decay' phase obeys an exponential law of the form:

$$h = h_0 + h_0(\beta - 1)\frac{1 - e((t - t_e)/\tau)}{1 - e(-t_e/\tau)} \tag{23}$$

where t is time in the past, h_0 is today's relief amplitude, t_e is the time of the end of the orogenic phase and τ is the erosional response time. τ is the time it takes for relief to decrease by a factor e. If τ is short in comparison to t_e, most of the relief reduction takes place during the period following the end of the orogenic phase; if τ is much greater than t_e, relief has decayed quasi-linearly since the end of the orogenic phase.

Can we use thermochronological data and/or their relationship to elevation to put constraints on the value of the parameter τ characterizing the rate at which relief decreases during the post-orogenic phase of a mountain belt? To answer this question, we have performed another series of numerical experiments in which the value of the parameter τ was systematically varied. As in the previous set of experiments, we have taken $t_e = 100$ Ma and assumed values for τ of 10, 20, 40, 100 Ma and ∞. The elastic plate thickness is set at 40 km. All other parameters are given the same value as in the previous set of runs. The results are shown in Figure 6 as age distributions along the same profile for the apatite He system (Figure 6a) and apatite fission track (FT) system (Figure 6b). The fission track ages are calculated from predicted thermal histories using the method of van der Beek *et al.* (1995). We have also computed age–elevation relationships along a narrow transect near the centre of the orogen. They are shown in Figure 7. The gain estimates and the values of β derived from them are summarized in Table II.

The age distribution appears to be similar for all model runs (Figure 6) except for a younging of the ages with increasing value of τ. That the ages are older for small values of τ is consistent with a rapid phase of relief reduction following the orogenic phase (100 Ma ago) during which rocks are rapidly exhumed to the surface and cross the closure temperature isotherm. That the minimum age computed for $\tau = \infty$ is approximately 50 Ma is also consistent with a linear decrease in relief of approximately 3–4 km in 100 Ma. The fission track ages have a similar distribution but are all older, consistent with an approximate closure temperature of 110 °C.

The slope of age–elevation transects measured along the narrow valley in the centre of the orogen (Figure 7) is strongly dependent on the assumed value for the erosional response time, τ. For small values of τ, corresponding to a rapid decay of the topography following the orogen constructive phase, the apparent exhumation rate are very high, approximately five times larger than the value predicted for a linear, steady decrease in topography over the past 100 Ma. Comparing the apparent exhumation rates derived from the slope of the age–elevation profiles 'collected' in the central valley (Figure 7) for the apatite He and apatite FT ages, one notices that for large values of τ, i.e. quasi-linear decrease in relief, the exhumation rate derived from both thermochronometers is almost identical. For small values of τ, i.e. corresponding to a rapid relief decay following the end of the orogenic phase, the exhumation rate obtained from the apatite He chronometer is almost twice as large as that derived from the apatite FT ages. This is somewhat counterintuitive as it would lead to the conclusion that the rate of exhumation increased between 100 and

Table II. Computed gain values, G_L and G_S, and corresponding relief loss amplitude, β^{-1}, for five model runs characterized by different values of the erosional response time, τ. Method 1 and method 2 are as in Table I. Age is the mean of the reset ages

	Method 1			Method 2			
τ (Ma)	G_L (Ma km^{-1})	G_S (Ma km^{-1})	β^{-1}	G_L (Ma km^{-1})	G_S (Ma km^{-1})	β^{-1}	Age (Ma)
10	–7·8	2·9	3·7	–8·8 ± 0·2	2·9 ± 0·4	4	95
20	–13·4	5·6	3·4	–15·2 ± 0·3	5·5 ± 0·7	3·8	92
40	–22·0	9·8	3·2	–25·1 ± 0·5	9·7 ± 1·3	3·6	86
100	–31·5	13·7	3·3	–36·7 ± 0·8	13·7 ± 1·9	3·7	78
∞	–38·3	15·3	3·5	–45·5 ± 1·1	15·6 ± 2·4	3·9	73

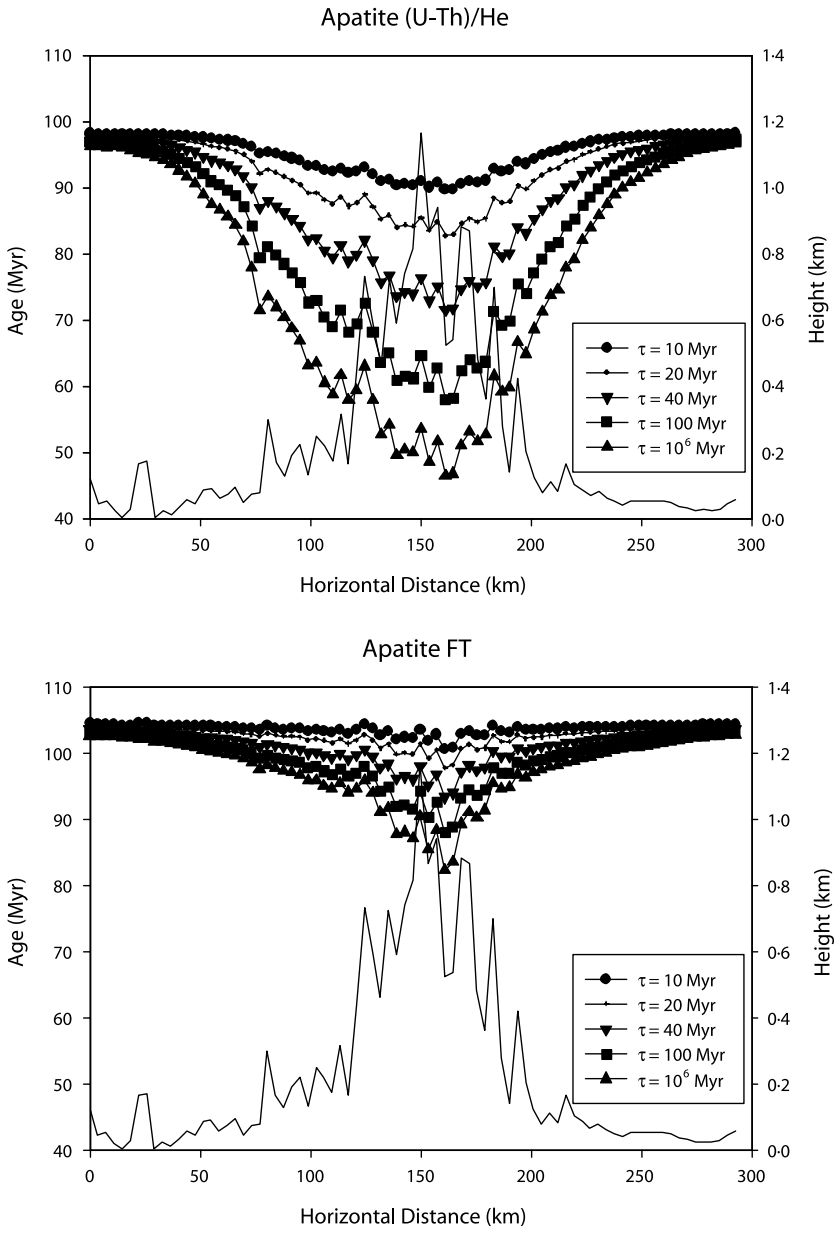

Figure 6. Topography and computed apatite He ages (a) and apatite FT ages (b) along a profile crossing the study area from the northwest to the southeast assuming different values for the erosional response time, τ.

90 Ma where, in fact, it decreased exponentially. This apparent increase in exhumation rate for the low temperature (and therefore younger) age estimates is a consequence of the rapid advection towards the surface which causes a greater perturbation to the closure temperature isotherm and generates higher apparent exhumation rates for the low temperature systems (Braun, 2002b).

Interestingly, the β-values derived from the gain estimates (Table II) are all consistent, regardless of the value of τ, indicating that the spectral method is very robust. Most estimates of β^{-1} are slightly smaller than the true value of 4. This is because by the time the rocks cools through the closure temperature for the apatite He system, the relief has already decrease by a small amount. The information contained in the age dataset can only provide us with information on the rate of relief change and/or mean exhumation rate since the time the rocks cooled through the closure temperature.

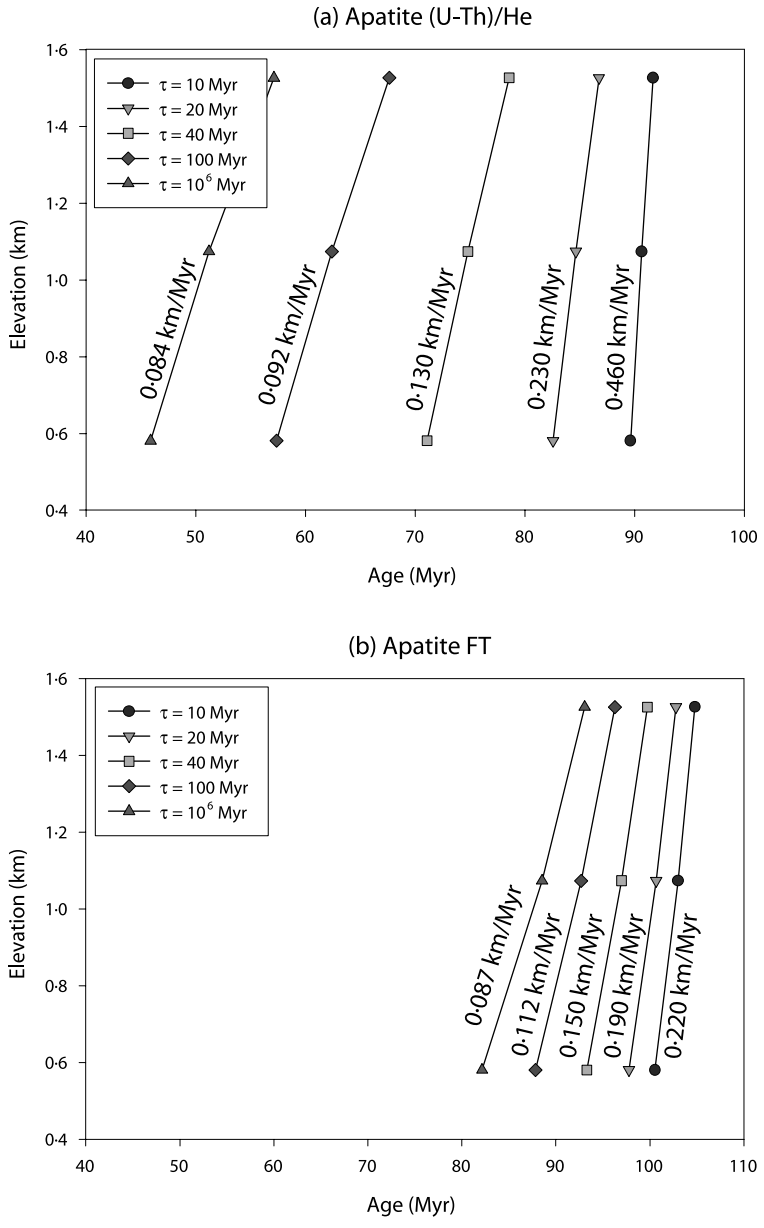

Figure 7. Computed apatite He age–elevation profiles from the centre of the orogen (Figure 4a). Each profile corresponds to a different value for the assumed erosional response time, τ. (a) (U-Th)/He system in apatite; (b) FT system in apatite.

In short, the slope of age–elevation profiles is sensitive to the rate at which erosional decay takes place during the post-orogenic phase of a mountain belt; estimates of the amount of relief/topographic change by the spectral method are not affected by the rate of decay, or whether it is linear or not.

Relief Evolution in the Dabie Shan

Spectral method

Having established that meaningful information about the rate of change of relief during the post-orogenic phase of mountain belt evolution can be extracted from thermochronological datasets, we turn our attention to the

data collected by Reiners *et al.* (2003) in the Dabie Shan (Figure 8). Our main purpose is to determine how the concepts illustrated by synthetic examples in the first part of this paper can be applied to a 'real' dataset. Rocks were collected across the orogen for (U-Th)/He and fission track dating in apatite and zircon (Reiners *et al.*, 2003). Here we focus on the low temperature, apatite datasets (Figure 8). In both datasets, there is a general trend of younger ages near the core of the orogen and older ages around its rim. An age–elevation transect collected near the centre of the orogen yields well-defined age–elevation relationships for the He dates with a slope, or apparent exhumation rate, of approximately 0·064 km Ma^{-1} and, for the FT dates, a slope of 0·042 km Ma^{-1}. This could be interpreted as indicating an increase in exhumation rate between 60 and 35 Ma ago, i.e. the mean age of each datasets. However, as discussed by Reiners *et al.* (2003), it is more likely that this apparent increase in exhumation rate is, in fact, related to the deflection of the closure temperature isotherm (approximately 55–75 °C for apatite He and 100–120 °C for apatite FT) by the surface topography. The valley in which the vertical transect was collected is approximately 12 km wide (Reiners *et al.*, 2003). It can be estimated that the deflection of the isotherm corresponding to the closure temperature for He in apatite caused by a 12-km-wide valley is sufficient to explain the difference in apparent exhumation rate. After correction, this yields a meaningful, orogen-wide exhumation rate of 0·06 km Ma^{-1} (Reiners *et al.*, 2003). It was thus shown by Reiners *et al.* (2003) that the dataset is consistent with a scenario in which the mean exhumation rate has not changed since the end of the large mid-Cretaceous exhumation event (i.e. approximately 100 Ma ago).

This dataset has not been collected with the purpose of using the spectral method of Braun (2002a) to interpret its significance in terms of mean exhumation rate and rate of landform evolution. This would have required the collection of samples along a single transect crossing the orogen and at nearly equidistant locations. However, one can obtain a first-order estimate of the long wavelength gain value by restricting the dataset to the samples located in a narrow corridor as done by Reiners *et al.* (2003, figure 1B) and projecting and interpolating both the observed ages and elevations onto a southwest–northeast transect to estimate their Fourier components. Using the apatite He age, we obtain a value of approximately −50 Ma km^{-1} for the real part of the gain estimate at long wavelength. The negative value simply indicates that there is an anti-correlation between age and elevation, which, following the arguments developed in Braun (2002a,b), implies that the long wavelength relief has decreased in the recent geological past. Combining this with a value of 1/0·064 Ma km^{-1} for the short wavelength gain, i.e. the inverse of the slope age–elevation relationship observed in the narrow, central valley, yields a value of approximately 4 for the amount of relief reduction experienced by this orogen over the past 60–70 Ma, i.e. since the end of the orogenic phase. Considering that the present-day relief in the Dabie Shan is approximately 1·5 km, this implies that the mountain range was approximately 6 km high in the mid-Cretaceous.

Parameter search

More information can be extracted from this dataset. We have seen in the previous sections that the distribution of ages within the orogen (i.e. as a function of the distance to the orogen's centre) and the relationship between age and elevation vary significantly as the assumed elastic plate thickness or the erosional timescale is varied. The forward model Pecube can be used to search through parameter space for an 'optimal' set of parameters that result in age predictions that are similar to the observed ages (within measurement error), and also to evaluate the sensitivity of the model predictions to the value of the input parameters. In other words, we wish to 'invert' the thermochronological dataset to provide constraints on a range of Earth processes (surface erosion, lithospheric strength, temperature structure within the crust, timing of tectonic events, etc.) and/or, more importantly, to determine whether the dataset contains information on each of these processes.

To perform this inversion, we have used the Neighbourhood Algorithm (NA) of Sambridge (1999), a Monte-Carlo-type inversion method that does not require the calculation of the derivatives of the forward model with respect to the model parameters in its search for a minimum of the misfit function between observations and model predictions. Instead, the NA navigates through the parameter space to find this minimum by making use of the natural neighbour and Voronoi diagram concepts. The misfit function is defined as the L_2-norm of the weighted difference between the observation vector, O, and the prediction vector, P:

$$\text{misfit} = \frac{1}{n}\sqrt{\sum_{i}^{n}\left(\frac{O_i - P_i}{\Delta O_i}\right)^2} \tag{24}$$

where n is the number of measured ages (31 in our case) and ΔO_i are the observational errors. A detailed description of the NA can be found in Sambridge (1999). The important point to remember is that NA performs an intelligent

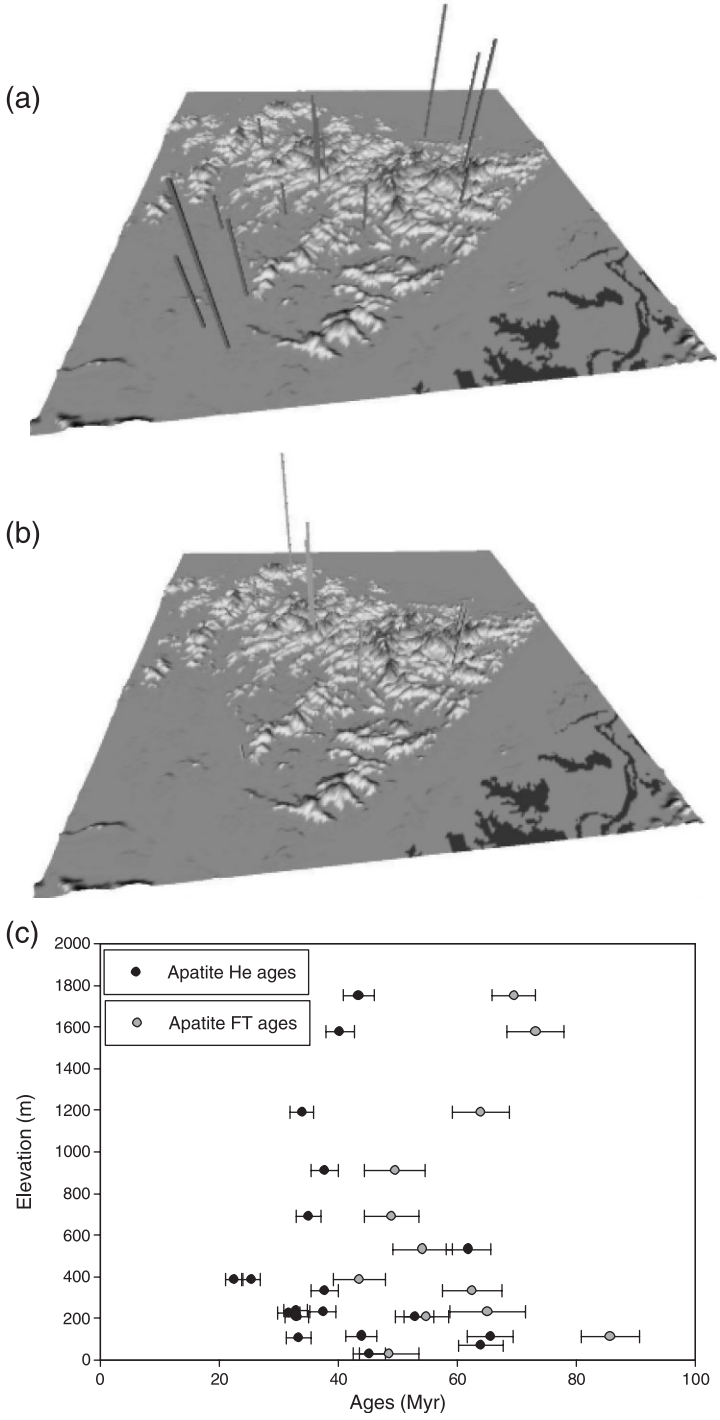

Figure 8. Relationship between age, topography and location for the apatite He dataset (a) and apatite FT dataset (b) collected by Reiners *et al.* (2003) in the Dabie Shan. Each bar corresponds to an age measurement. The location of the bar gives the location of the sample; the height of the bar is proportional to the measured age. Maximum age for apatite He is 65·5 Ma; maximum age for apatite FT is 85·7 Ma. (c) Age–elevation plot for apatite He and apatite FT ages. The relatively well-defined positive correlation between age and elevation among some of the data points corresponds to the vertical transect collected in the central part of the orogen; at the scale of the orogen, there is a negative correlation between age and elevation, with younger ages near the centre and older ages around the edges of the orogen.

search to find the set of parameter values of a given model (here Pecube) that will minimize the difference between model predictions (the synthetic ages) and observations (the measured ages). This search necessitates that a large number of model (Pecube) runs be performed to sample a wide range of parameter values.

In our application, the 'free' model parameters, i.e. those for which the inversion is performed, are the effective elastic plate thickness, L_e, the length of the model run, t_e, which can also be regarded as the time since the last major tectonic event at the end of which the erosional decay episode started, the erosional response time, τ, the basal temperature, T_1, the amplitude of the topography/relief decrease since the end of the orogenic phase, β^{-1}, and a mean exhumation rate, $\dot{E}$, i.e. uniform in space and constant in time.

Using a high performance cluster, we were able to perform a very large number of forward model runs (17 744 in total) in a reasonable amount of time. The results are shown in Figures 9 and 10 as scatter plots in parameter space. Each circle corresponds to a Pecube forward model run. The grey shade of the circles is proportional to the predicted misfit (dark shades correspond to low misfit, light shades correspond to high misfit). In Figure 9, all model runs are shown. In Figure 10, only the 50 best-fitting model runs are shown. Although the search was performed in a six-dimensional space (the space of the free parameters), we can only display the results as two-dimensional plots, by projecting the other four dimensions. We selected six combinations of pairs of parameters.

The results demonstrate that the thermochronological data contain information on: the timing of the end of the orogenic phase: 60 Ma $< t_e <$ 80 Ma; the effective elastic plate thickness: $L_e <$ 20 km; the amplitude of the relief loss: $2 < \beta^{-1} < 4$; the mean exhumation rate: 0·01 km Ma^{-1} $< \dot{E} <$ 0·04 km Ma^{-1}. The data do not contain information on the basal temperature, T_1, or the erosional response time, τ. The best-fitting forward model run (indicated on Figure 9 by a large white circle) is obtained with the following parameter values: $L_e = 9{\cdot}3$ km, $t_e = 72$ Ma, $\tau = 270$ Ma, $T_1 = 660$ °C, $\beta^{-1} = 2{\cdot}3$ and $\dot{E} = 0{\cdot}022$ km Ma^{-1}. The ages predicted from this best-fitting model run are shown and compared to the observed ages in Figure 11 as age–elevation distributions for the He and FT ages. The best forward model run is able to explain the steep, positive correlation between age and elevation near the centre of the orogen and the increase in age with distance from the centre of the orogen (and thus mean elevation). For the value of the 'best fit model' parameters, the total erosion in the centre of the orogen is approximatively 4 km, i.e. 1·6 km of uniform erosion, 2 km of relief loss and 0·4 km of associated isostatic rebound. That the data are better explained by a model in which a mean rock exhumation of 0·022 km Ma^{-1} is imposed indicates that areas where little surface topography exists today have undergone finite exhumation/erosion. We interpret this result as indicating that our approximation of relief evolution by simple amplification (or multiplication) is too simplisitic.

One should note, however, that the 'best' 50 model runs differ by less than 4 per cent in their misfit to the data but differ markedly by the value of the model parameters. The location in parameter space of these 50 best-fitting model runs is shown in Figure 10. Their distribution demonstrates that some of the model parameters are linearly dependent, i.e. that there is a trade-off between pairs of parameters: the data are equally explained by high relief loss or low mean exhumation rate (and vice versa) (see Figure 10c); the data are equally explained by high elastic thickness or high mean exhumation rate (and vice versa) (see Figure 10e); the data are consequently equally explained by high relief loss or high elastic plate thickness (and vice versa) (see Figure 10d). The timing of the end of the orogenic phase is independent of the other parameters.

The results of the inversion confirm the conclusions of Reiners *et al*. (2003) that, to explain the thermochronological data, there is no need to invoke a discrete tectonic event some 40–60 Ma ago as suggested by Grimmer *et al*. (2002). Slow exhumation related in part to the erosional decay of a relatively large surface topography and the subsequent isostatic uplift can explain the data. Surface topography/relief appears to have decreased by a factor of 2 to 4 since the beginning of the erosional decay phase. The data are better explained, however, if one assumes that the entire orogen (including the present-day low topography areas) has undergone, in addition to the isostatically driven exhumation, 1·6 km of uniform exhumation. Interestingly, the thermochronological data appear to provide better constraints on the effective elastic thickness of the underlying lithosphere than on the temperature structure (i.e. geothermal gradient) of the crust.

Finally, the results of the inversion (Figures 9 and 10) suggest that there is little information in the data to determine whether the relief loss occurred soon after the end of the orogenic event (small value of τ) or whether the topography has decayed at a constant rate since (large value of τ). However, most of the best-fitting model runs are characterized by relatively large values of τ, i.e. larger than 100 Ma, suggesting that a linear decrease in topographic height over the past 60–70 Ma is the most likely scenario. In Figure 12, we compare observations with predicted ages for a model run characterized by a small value of the erosional reponse time, $\tau = 16{\cdot}5$ Ma. Other parameters are $L_e = 12{\cdot}4$ km, $t_e = 73$ Ma, $T_1 = 600$ °C, $\beta^{-1} = 2{\cdot}5$ and $\dot{E} = 0{\cdot}028$ km Ma^{-1}. It is the sixth best-ranked model and is shown as a dark black circle in Figure 10. The predicted ages (Figure 12) have similar age–elevation slope to the observations but the He ages are clearly older than the observations, suggesting that a small value (i.e. smaller than 100 Ma) for τ is not compatible with the data.

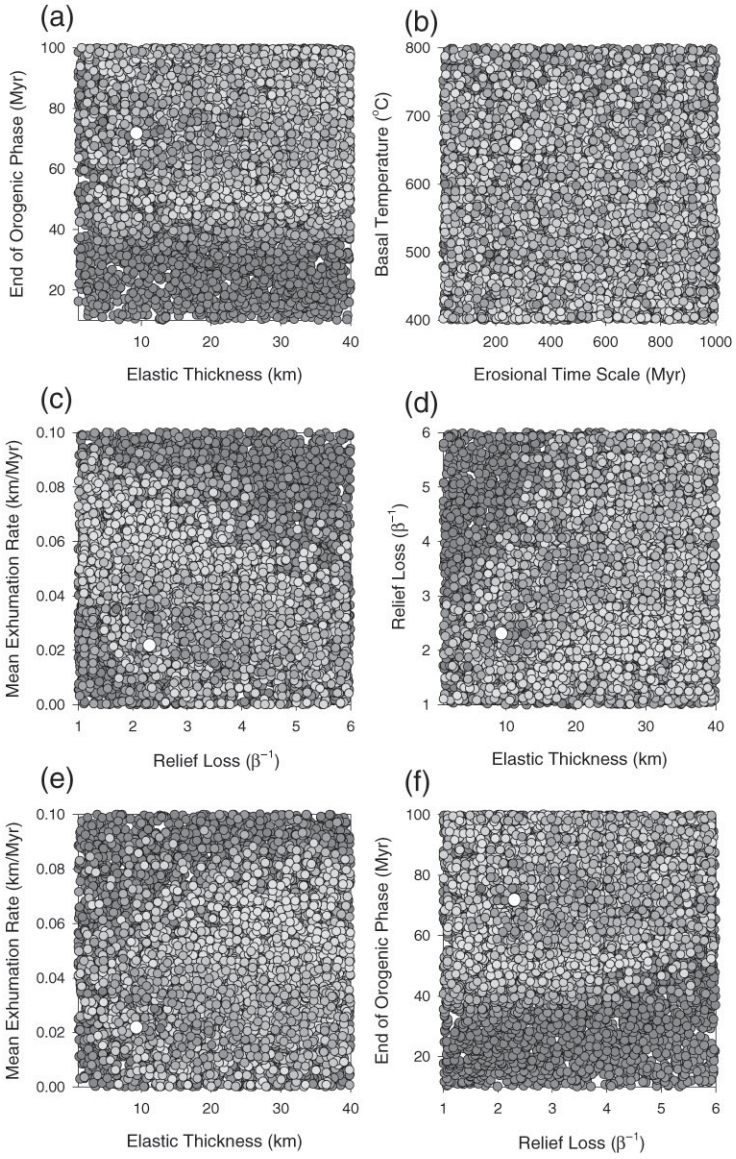

Figure 9. Results of the NA inversion as scatter diagrams of the misfit between observations and predictions. Each circle corresponds to a forward model run. The position of the circle is determined by the value of the model parameters. The grey shade of the circle is proportional to the value of the calculated misfit: dark shades correspond to low misfit values; light shades corresponds to high misfit values. The larger, white circle corresponds to the best-fit model run. Each diagram corresponds to a projection of all model runs onto a plane defined by two of the six parameters. Note that during the inversion procedure all model parameters are free to vary simultaneously. Only a small number (six) of all possible combinations of pairs of parameters are shown.

Conclusions and Discussion

Using a numerical model for the evolution of the temperature structure within the Earth's crust that includes the effect of a changing, finite-amplitude surface topography and isostatically driven exhumation, we have demonstrated that thermochronological data can be used to put constraints on the rate and amplitude of topographic decay during the post-orogenic phase of mountain belt evolution.

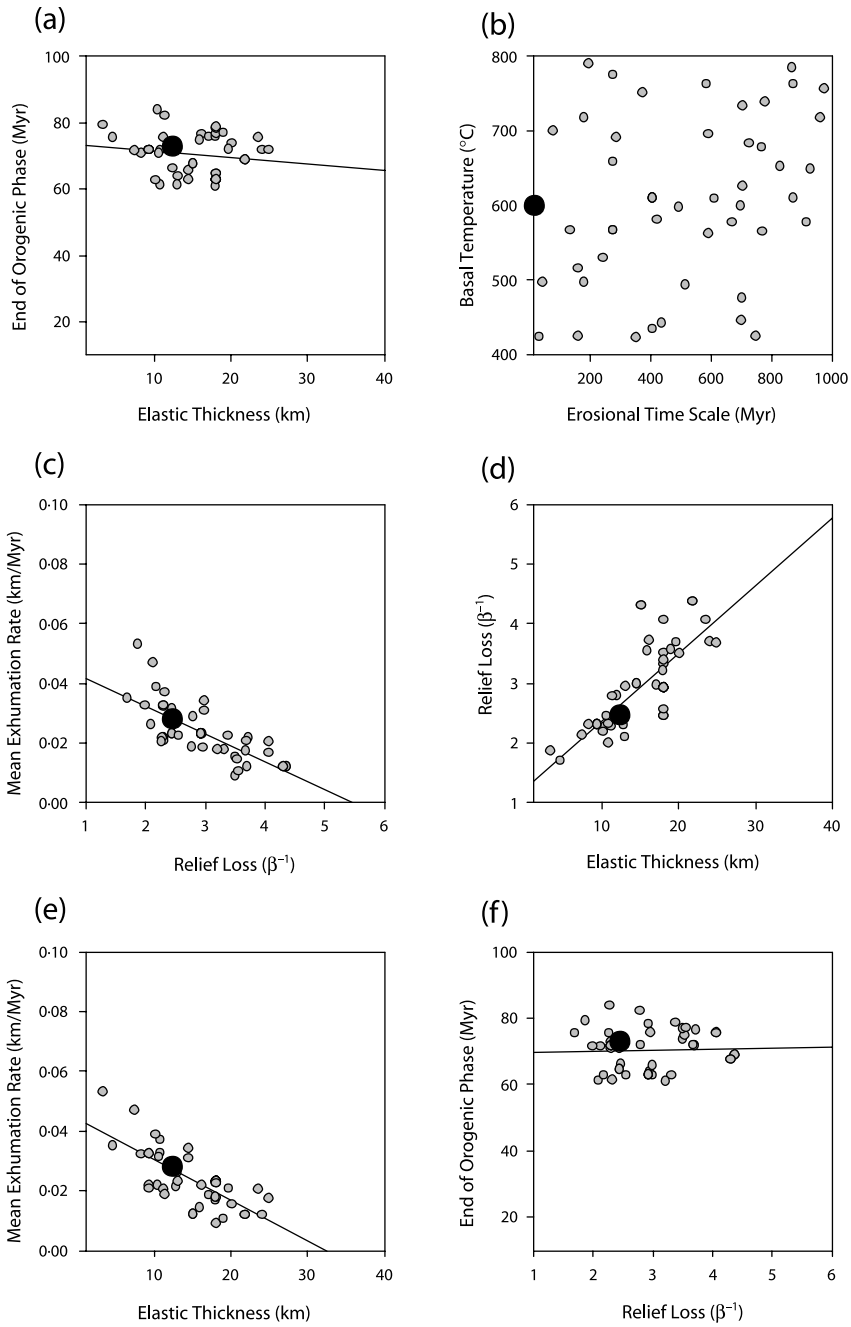

Figure 10. Same as Figure 9 but limited to the 'best' 50 model runs, i.e. those corresponding to the 50 smallest misfit values out of the 17 744 model runs performed during the inversion procedure with NA. The larger, black circle corresponds to the sixth best-fit model run, characterized by a small value of the parameter τ.

In particular, the spectral method developed by Braun (2002a) provides very good estimates of the mean exhumation rate and amplitude of relief loss even in cases when erosion is controlled by flexural isostasy; it is only in cases where lithospheric strength is so low and the effective elastic thickness is of the order of a few kilometres or less that the method overestimates the amount of relief loss.

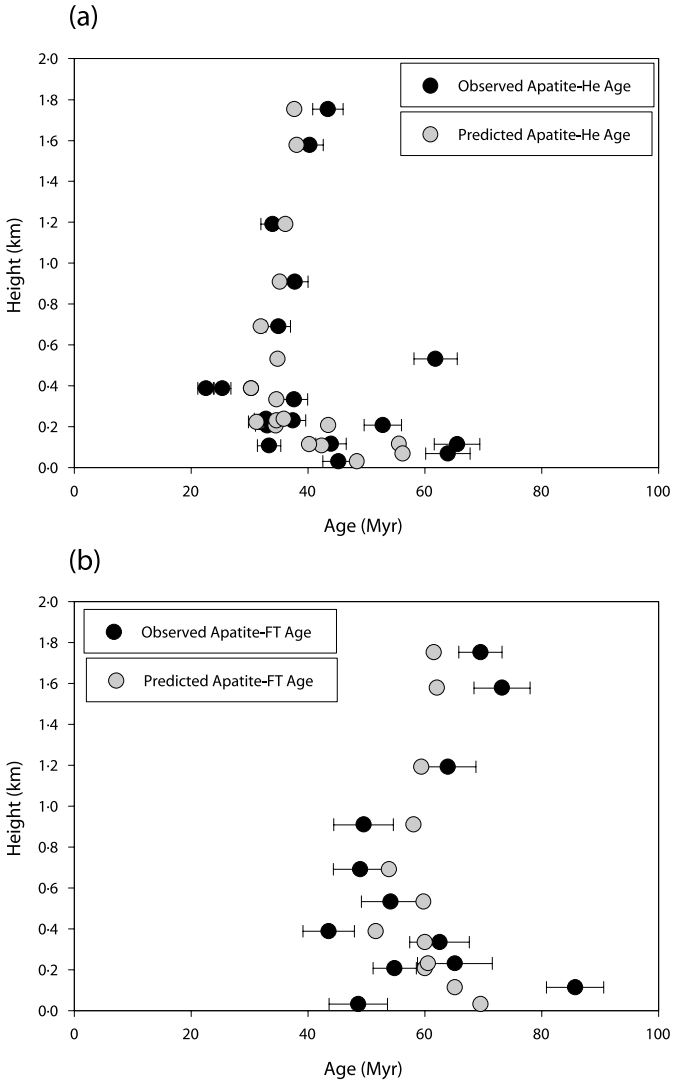

Figure 11. Comparison between observed and synthetic age–elevation relationships for apatite He ages (a) and apatite FT ages (b) estimated from the best-fitting model run.

The timescale, τ, over which relief decays once tectonic activity ceases can also be constrained by low-T thermochronological data; the slope of age–elevation profiles collected along short wavelength topography provides a good estimate of the mean rate of erosion which, in turn, is strongly dependent on the mean rate of topographic decay.

Applying the spectral method to a thermochronological dataset collected in the Dabie Shan of eastern China provides first-order estimates of the amount of relief reduction ($\beta^{-1} = 4$) since the end of tectonic activity (at least 70 Ma ago).

A thorough search through parameter space indicates that the Dabie Shan dataset is best explained if the underlying lithospheric thickness if of the order of 10 km, the relief has decreased by a factor of approximately 2·5 over the last 60 to 70 Ma, and if the area has been subjected, over the same period of time, to a mean exhumation rate of 0·02 km Ma^{-1}.

We have also demonstrated that these optimum parameter values should not be regarded as unique; the data suggest that there is a trade-off between mean exhumation rate and relief loss. For example a smaller mean exhumation rate of 0·01 km Ma^{-1} and a greater relief loss of 4·5 leads to a misfit to the data that is only a few per cent greater than that calculated for the optimum parameter set. There is also a trade-off between elastic thickness and relief loss with model

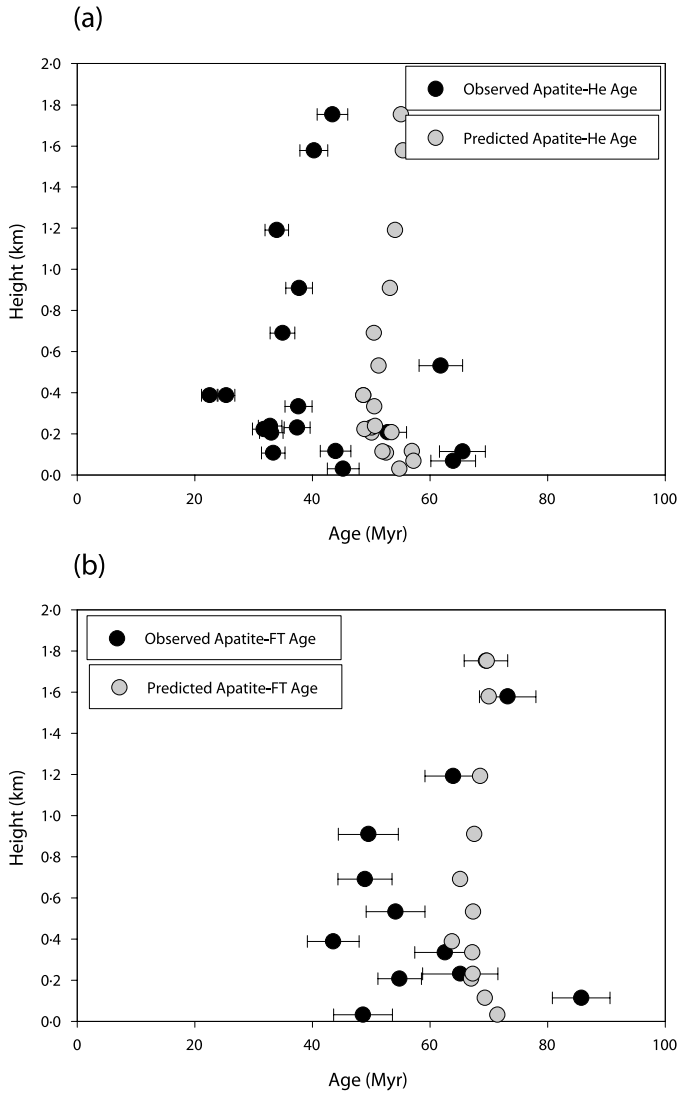

Figure 12. Comparison between observed and synthetic age–elevation relationships for apatite He ages (a) and apatite FT ages (b) estimated from the sixth best-fitting model run, characterized by a small erosional response time, $\tau = 16{\cdot}5$ Ma.

runs characterized by a larger elastic thickness (up to 30 km thick) and a greater topographic relief loss (up to 4·5) yielding similar misfit values.

We also found that surface topography in the Dabie Shan is likely to have decayed relatively linearly since the end of the orogenic event; the value for the parameter τ cannot be accurately derived from the thermochronological dataset but is likely to be relatively large, i.e. $\tau > 100$ Ma.

Finally, the misfit between model predictions and observations appears insensitive to the choice of geothermal gradient.

The most interesting result of our analysis of the Dabie Shan dataset is that it supports the conclusion of Reiners *et al*. (2003) that the rate of exhumation and thus the rate of change of surface topography has been more or less constant during the post-orogenic phase of the evolution of the mountain belt. The 'best-fit model' is not compatible with an exponential decrease in relief (and thus erosion rate) as predicted by most landscape evolution models that assume that the rate of erosion is proportional to relief amplitude (through the slope dependency of most erosional processes).

This result can be interpreted in several ways.

(1) The large-scale features of the landform do not evolve at a rate that is proportional to their relative height. This would imply that although the basic physical processes that drive the evolution of surface topography through time, such as stream incision or hill slope processes, have a strong dependency on local slope, this cannot later be time-averaged or spatially homogenized at the scale of an orogen and lead to a dependency of mean erosion rate on the slope measured along its major large-scale features. This would then imply that much of the recent work on the balance between tectonics and erosion that is based on an extrapolation of the stream power law to the overall shape of an orogen (Hilley and Strecker, 2004; Roe *et al*., 2005; Whipple and Meade, 2004) is not well posed.
(2) Other landforming processes, such as glacial erosion, may play a more important role than commonly assumed (Braun *et al*., 1999; Tomkin and Braun, 2002) and lead to a constant lowering rate, especially in mountainous regions that are in a post-orogenic erosional decay phase.
(3) Low-*T* thermochronological data are not sufficiently sensitive to changes in surface relief to provide constraint on the details of the temporal evolution of the relief. This does not seem to be supported by the results of our modelling (Figures 6 and 7) but could be due to the accuracy with which small variations in ages can be recorded by and extracted from the rocks.

Acknowledgements

The results presented in this paper are based on computations performed on the TerraWulf facility of the Centre for Advanced Data Inference of the Australian National University, in part funded by an Australian Research Council grant. The authors wish to thank P. Reiners and an anonymous reviewer for their helpful comments on an earlier version of this manuscript.

References

Bechtel T, Forsyth D, Sharpton V, Grieve R. 1990. Variations in effective elastic thickness of the North American lithosphere. *Nature* **343**: 636–638.

Braun J. 2002a. Estimating exhumation rate and relief evolution by spectral analysis of age–elevation datasets. *Terra Nova* **14**: 210–214.

Braun J. 2002b. Quantifying the effect of recent relief changes on age–elevation relationships. *Earth and Planetary Sciences Letters* **200**: 331–343.

Braun J. 2003. Pecube: A new finite element code to solve the heat transport equation in three dimensions in the Earth's crust including the effects of a time-varying, finite amplitude surface topography. *Computers and Geosciences* **29**: 787–794.

Braun J, Zwartz D, Tomkin J. 1999. A new surface processes model combining glacial and fluvial erosion. *Annals of Glaciology* **28**: 282–290.

Davis W. 1899. The geographical cycle. *Geography and Geomorphology Journal* **14**: 481–504.

Dodson MH. 1973. Closure temperature in cooling geochronological and petrological systems. *Contributions to Mineralogy and Petrology* **40**: 259–274.

Forsyth D. 1985. Subsurface loading and estimates of the flexural rigidity of continental lithosphere. *Journal of Geophysical Research* **90**: 12 623–12 632.

Grimmer J, Jonckheere R, Enkelmann E, Rauschbacher L, Hacker B, Blythe A, Wagner G, Wu Q, Liu S, Dong S. 2002. Cretaceous-Cenozoic hidtory of the southern Tan-Lu fault zone: apatite fission-track and structural constraints from the Dabie Shan (eastern China). *Tectonophysics* **359**: 225–253.

Hack T. 1960. Interpretation of erosional topography in humid temperate regions. *American Journal of Science* **258A**: 80–97.

Hilley G, Strecker M. 2004. Steady-state erosion of critical Coulomb wedges with application to Taiwan and the Himalaya. *Journal of Geophysical Research* **109**. DOI: B01411–10.1029/2002JB002284.

Huang J, Turcotte D. 1989. Fractal mapping of digitized images: application to the topography of Arizona and comparisons with synthetic images. *Journal of Geophysical Research* **94**: 7491–7495.

Jenkins GM, Watts DG. 1968. *Spectral Analysis and its Applications*. Holden-Day: Oakland, California.

Kooi H, Beaumont C. 1996. Large-scale geomorphology: classical concepts reconciled and integrated with contemporary ideas via a surface processes model. *Journal of Geophysical Research* **101**: 3361–3386.

Lague D, Crave A, Davy P. 2003. Laboratory experiments simulating the geomorphic response to tectonic uplift. *Journal of Geophysical Research* **108**. DOI: 10.1029/2002JB001785.

Maggi A, Jackson J, McKenzie D, Priestley K. 2000. Earthquake focal depths, effective elastic thickness, and the strength of the continental lithosphere. *Geology* **28**: 495–498.

Molnar P, England P. 1990. Late Cenozoic uplift of mountain ranges and global climate change: chicken and egg? *Nature* **346**: 29–34.

Montgomery DR. 1994. Valley incision and the uplift of mountain peaks. *Journal of Geophysical Research* **99**: 13 913–13 921.

Nunn J, Aires J. 1988. Gravity anomalies and flexure of the lithosphere at the Middle Amazon Basin, Brazil. *Journal of Geophysical Research* **93**: 415–428.

Penck W. 1924. *Die Morphologische Analyse: Ein Kapital der Physikalischen Geologie*. Engelhorn: Stuttgart.

Reiners P, Zhou Z, Ehlers T, Xu C, Brandon M, Donelick R, Nicolescu S. 2003. Post-orogenic evolution of the Dabie Shan, eastern China, from (U-Th)/He and fission-track thermochronology. *American Journal of Science* **303**: 489–518.

Roe G, Stolar D, Willett S. 2005. The sensitivity of a critical wedge orogen to climatic and tectonic forcing. In *Tectonics, Climate, and Landscape Evolution*, Willett S, Hovius N, Brandon M, Fisher D (eds). GSA Special Publication.

Sambridge M. 1999. Geophysical Inversion with a Neighbourhood Algorithm -I. Searching a parameter space. *Geophysical Journal International* **138**: 479–494.

Schmid R, Ryberg T, Ratschbacher L, Schulze A, Franz L, Oberhansli R, Dong S. 2001. Crustal structure of the eastern Dabie Shan interpreted from deep seismic reflection and shallow tomographic data. *Tectonophysics* **333**: 347–359.

Stüwe K, White L, Brown R 1994. The influence of eroding topography on steady–state isotherms. Application to fission track analysis. *Earth and Planetary Sciences Letters* **124**: 63–74.

Tomkin J, Braun J. 2002. The effect glaciation has on the relief of a fast growing orogen: a numerical modelling study. *American Journal of Science* **302**: 169–190.

Turcotte D. 1979. Flexure. *Advances in Geophysics* **21**: 51–86.

Turcotte DL, Schubert G. 1982. *Geodynamics: Applications of Continuum Physics to Geological Problems*. John Wiley and Sons: New York.

van der Beek P, Andriessen P, Cloetingh S. 1995. Morpho-tectonic evolution of rifted continental margins: Inferences from a coupled tectonic–surface processes model and fission-track thermochronology. *Tectonics* **14**: 406–421.

Wang Y, Mareschal J-C. 1999. Elastic thickness of the lithosphere in the Central Canadian Shield. *Geophysical Research Letters* **26**: 3033–3035.

Whipple K, Meade B. 2004. Controls on the strength of coupling among climate, erosion, and deformation in two-sided, frictional orogenic wedges at steady state. *Journal of Geophysical Research* **109**: F01011. DOI: 10.1029/2003JF000019.

Whipple KX, Tucker G. 1999. Dynamics of the stream-power incision model: implications for height limits of mountain ranges, landscape response timescales and research needs. *Journal of Geophysical Research* **104**: 17 661–17 674.

Wolf RA, Farley KA, Kass DM. 1998. Modeling of the temperature sensitivity of the apatite (U-Th)/He thermochronometer. *Computers and Geosciences* **148**: 105–114.

Zuber M, Bechtel T, Forsyth D. 1989. Effective elastic thickness of the lithosphere and mechanisms of isostatic compensation in Australia. *Journal of Geophysical Research* **94**: 9353–9367.

